Deep Resources Engineering 3 (2026) 100207

Contents lists available at ScienceDirect

Deep Resources Engineering

journal homepage: www.keaipublishing.com/en/journals/deepre/

Full length article

Infrared thermal image detection method of stressed sandstone fracture based on deep learning

Hai Sun [a,b,c,*], Xinyi Hou [a], Liqiang Ma [b,c], Wenshuang Gao [a], Kun Wang [a]

[a] School of Civil Engineering, Liaoning Petrochemical University, Fushun, Liaoning 113001, China
[b] Key Laboratory of Xinjiang Coal Resources Green Mining (Xinjiang Institute of Engineering), Ministry of Education, Urumqi 830023, China
[c] Xinjiang Engineering Research Center of Green Intelligent Coal Mining, Xinjiang Key Laboratory of Coal-bearing Resources Exploration and Exploitation, Xinjiang Institute of Engineering, Urumqi 830023, China

ARTICLE INFO

Keywords:
Rock mass
Crack
Infrared thermal imaging
Convolutional attention mechanism
Deep learning

ABSTRACT

Under stress, multiple cracks in the localized damaged zones in mine rock masses will expand and connect, which can lead to the rock mass instability and failure. Rapid, accurate identification of cracks within damaged zones forms a critical foundation for predicting and preventing rock mass fracture instability. To address the need for non-contact precise measurement of mine rock mass fractures, this study proposes an automated method for detecting and identifying fractures in infrared thermal images using deep convolutional neural networks. First, infrared thermal images containing temperature anomalies during sandstone fracturing are captured via infrared thermal imaging. Next, deep learning is used to develop sandstone fracture detection models for infrared thermal images based on the SSD and YOLOv5 algorithms. Compared to the YOLOv5 algorithm, the SSD algorithm detects sandstone fracture regions with higher accuracy and confidence. Building on this, a convolutional attention mechanism is integrated to optimize the SSD algorithm. The optimized algorithm achieves 90.2 % detection accuracy for successive difference infrared thermal images, with improved precision in sandstone fracture detection. The research results can provide the development of computer vision-based fracture detection technologies for stressed rock masses.

1. Introduction

As shallow resources become increasingly depleted, deep mining has emerged as a critical strategic scientific and technological challenge for China. Upon entering deep mining zones, the geological environment becomes complex, and rock dynamic disasters occur frequently. Fracture development in stressed coal and rock masses is a key factor contributing to their damage, while the rapid and accurate identification of fractures forms an important basis for predicting and preventing rock fracture instability [1–5]. During the development of fractures in coal and rock masses, infrared radiation effects are generated, and the regions where such fractures occur can be identified by analyzing the characteristics of infrared radiation parameters. Wu et al. [6–8] conducted a preliminary study on the damage precursors of coal and rock masses, finding that these materials exhibit three types of infrared thermal image characteristics and three types of infrared radiation temperature characteristics during the loading process. Liu et al. [9] employed quantitative characterization indices, including the average infrared radiation temperature on coal and rock surfaces, and the maximum and minimum radiation temperatures in infrared thermal image sequences, to quantitatively analyze the relationship between infrared radiation characteristics and coal-rock failure precursors. Li et al. [10] used infrared thermography to obtain the state of crack expansion during loading damage. Wu et al. [11] proposed the concept of "infrared temperature field" and discussed the characteristics of the infrared temperature field transient changes during rock fracture instability. Ma et al.[12] proposed a temperature variance method for differential infrared thermal image sequence maps based on the original infrared thermal image sequence maps, which improved the accuracy of the infrared radiation characteristics of coal and rock. Liu et al. [13]used infrared thermography to study rock damage and damage precursors. Zhou et al. [14] analysed the evolutionary characteristics of infrared thermal images and the change rule of the average infrared radiation temperature of sandstone under different loading rates. In practical applications, infrared thermography still encounters challenges. It often relies on manual and subjective identification of thermal anomalies

* Corresponding author at: School of Civil Engineering, Liaoning Petrochemical University, Fushun, Liaoning 113001, China
E-mail address: sunhai@lnpu.edu.cn (H. Sun).

https://doi.org/10.1016/j.deepre.2025.100207
Received 20 May 2025; Received in revised form 15 July 2025; Accepted 22 July 2025
Available online 26 July 2025

within infrared thermograms to pinpoint rock mass fracture locations. This methodology, however, significantly compromises fracture recognition accuracy. Consequently, enhancing the recognition precision of rock mass fractures utilizing infrared thermographic information remains an area requiring further investigation. Deep learning, notably capable of unsupervised training and extracting salient features from complex nonlinear functions, has been widely applied in image processing and presents potential solutions.

In recent years, scholars have begun to try to introduce deep learning techniques into the field of rock crack detection. Zhang et al. [15] studied the strain field evolution process during the destruction of complex fractured rocks based on the YOLO deep learning network model while combining the digital image correlation (DIC) method, and proposed an algorithm for intelligent and accurate identification of dynamic fractures. Xu et al. [16] explored the applicability of these two algorithms under different forms of tunnel face fracture through the comparison of two algorithms, namely, the Faster R-CNN and the Mask R-CNN. By comparing Faster R-CNN and Mask R-CNN algorithms, the applicability of these two algorithms in different forms of cleavage in the tunnel face is explored. Yuan et al. [17] used the DeepLabv3 + algorithm to construct a deep convolutional neural network, and used MobileNetV2 as the main feature extraction network to establish a detection and segmentation framework for "long line" and "curved" fractures in coal roadway excavation working faces, achieving accurate detection of these fractures. With the advancement of deep learning in object detection, integrating deep learning with infrared thermography for non-destructive testing of damage fracture zones in loaded coal-rock masses has emerged as a prominent research trend. Lu [18] proposed a detection model for differentiating tensile-shear cracks in rock infrared thermograms, which enables identification of fracture modes during material failure. Huang [19] used the improved Faster R-CNN model to process the infrared thermal images of rock cracks, and effectively detected and localized the crack areas and their coordinates. Furthermore, Jang et al. [20] combined the deep convolutional neural network GoogLeNet with infrared thermal images to achieve the automatic visualization of macroscopic and microscopic cracks in concrete. Li [21] proposed an improved SSD model, which reduces the computational complexity of the model while improving the detection accuracy of small infrared targets. Chen [22] proposed a target detection model based on YOLOv5, which can realize dynamic fracture detection and recognition for fractured rock specimens. Zhao et al. [23] proposed a method for segmenting abnormal areas in infrared thermal images of coal based on a multi-scale channel attention module, which can identify damaged areas.

The aforementioned studies take original infrared images as the research object. However, these original infrared images exhibit significant background noise, which substantially interferes with accurate and effective detection of fracture zones, inevitably leading to false detection and missed detection of fractures. Existing algorithms exhibit insufficient accuracy in detecting small-sized targets, thus requiring optimization in combination with application scenarios to improve the detection accuracy of small fractures. Based on this, this paper carries out infrared radiation tests of loaded sandstone, collects infrared radiation images of sandstone, and constructs a dataset of sandstone infrared thermal images. The SSD and YOLOv5 algorithms were used to establish the infrared thermal image detection model of the loading sandstone cracks, and were trained on the dataset to detect the infrared thermal images during the whole process of loading sandstone samples. On this basis, the convolutional attention mechanism is introduced to optimize the algorithm model, which improves the detection of small cracks in the infrared thermal images and provides a reference basis for the development of computer vision-based crack detection technology for stressed rock bodies.

2. Experimental design

2.1. Test rock samples and equipment

The test samples were taken from the same rock body and processed into cylindrical rock samples with a diameter of 50 mm and a height of 100 mm, totaling 12 specimens, numbered Ai ($i = 1$–12). The hydraulic servo-controlled testing machine MTS C64.106 was used for uniaxial compression tests. This device offers a maximum axial test force of 1000 kN, with a test force measurement accuracy of ±0.5 %. The infrared monitoring equipment was a VarioCAM HD head 880 infrared camera with a temperature range of −40 ~ 1200 °C, a resolution of 1024 × 768, and a spectral range of 7.5 ~ 14 μm.

2.2. Test methods

The infrared camera was set up at a position 1 m directly in front of the sample (as shown in Fig. 1). Movement in the laboratory was strictly prohibited to minimize interference. The test employed constant displacement loading at a 0.2 mm/min loading rate, and the acquisition rate of the infrared camera was 10 frames per second.

2.3. Infrared thermal imaging index

The original infrared thermal image can reflect the infrared radiation information and temperature distribution during the loading process of the sample. Fig. 2 shows the original infrared thermal images of the sandstone A7 sample at various stages. The successive difference infrared thermal image is obtained from the original infrared thermal image by the first-order forward difference method, which can reflect the spatial distribution difference between the original infrared thermal image of a certain frame of the sample and the previous frame of the original infrared thermal image, so as to find out the characteristics of the transient infrared radiation changes. The two-dimensional temperature matrix of the p^{th}-frame successive difference infrared image is:

$$\varphi_p(x,y) = f_{p+1}(x,y) - f_p(x,y) \tag{1}$$

Where $f_p(x,y)$ is the two-dimensional temperature matrix of the p^{th}-frame original infrared thermal image; x and y represent the row and column numbers of the temperature matrix of the camera, respectively. Fig. 3 shows the successive difference infrared thermal images of the sandstone A7 sample at various stages.

3. Infrared thermal image detection model for sandstone fractures

3.1. Dataset establishment

The 236 original and successive difference infrared thermal images with temperature anomalies were selected, and the number of training samples was increased by angular transformations, flipping, and scale transformations of the images, so that the number of training samples of

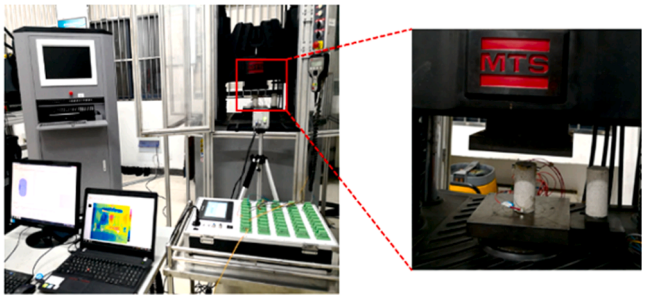

Fig. 1. Test system.

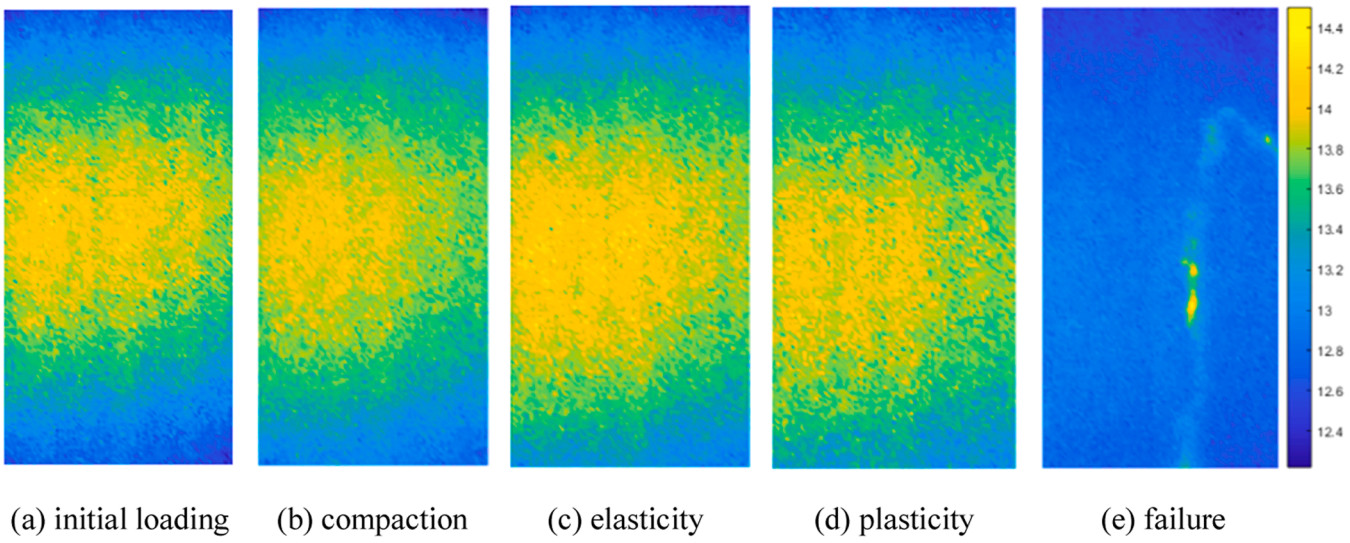

Fig. 2. The original infrared thermal image changes of sample A7.

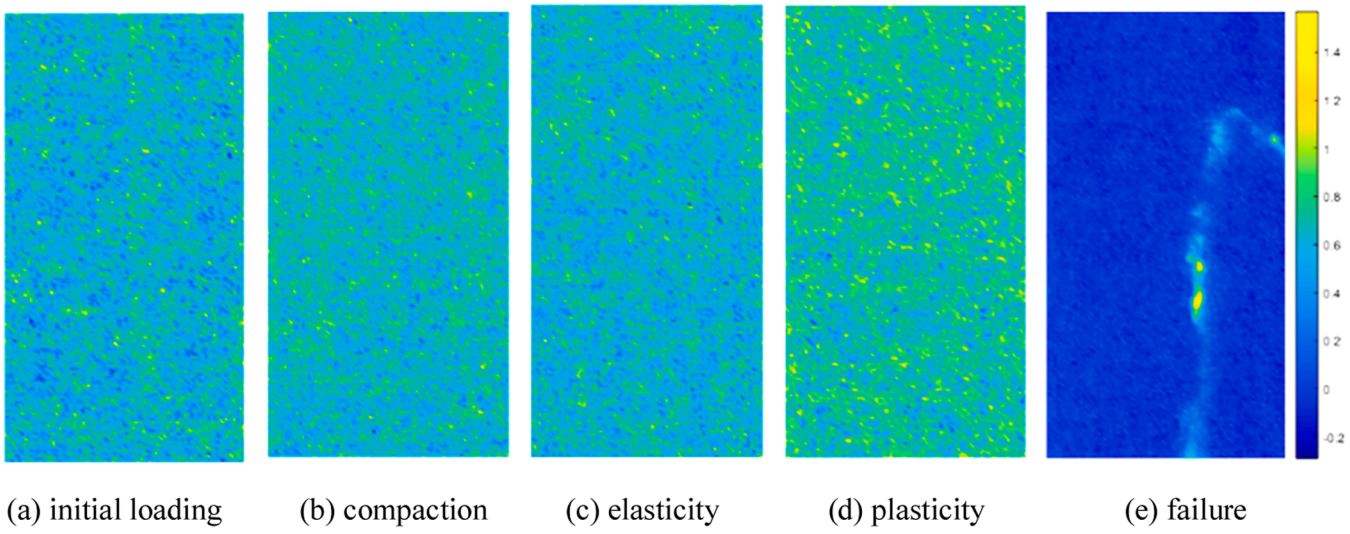

Fig. 3. The successive difference infrared thermal image changes of sample A7.

each type was expanded to 3000. According to the PASCAL VOC2012 dataset specification, the infrared thermal image dataset containing the information of crack labeling was produced, and the LabelImg software was used to label the cracks in detail, indicating their types and related information. Each dataset was randomly divided into two parts, 90 % as the training set and 10 % as the test set. The dataset of infrared thermal images is shown in Fig. 4.

3.2. Model training

Considering the model's requirement for strong fitting capability, high accuracy, and rapid detection, this paper chooses the one-stage algorithm represented by SSD and YOLOv5, which can improve the detection speed while ensuring the detection accuracy rate, and is more in line with the detection requirements of infrared thermal images.

(1) SSD algorithm model

The SSD network is constructed by replacing the two fully connected layers after Conv5 in the VGG network model with two convolutional layers, and then adding Conv8, Conv9, Conv10, and Conv11 after fc7 [21]. The structure diagram of SSD algorithm model is shown in the Fig. 5.

(2) YOLOv5 algorithm model

The YOLO series algorithms are widely used in the field of object detection. Among them, YOLOv5 can ensure the accuracy of test results during the research process, while also having good compatibility with various hardware platforms, which greatly reduces the difficulty of hardware adaptation [24]. The structure diagram of YOLOv5 algorithm model is shown in the Fig. 6.

The model training was carried out in the PyCharm development environment, and the framework is PyTorch 1.9. The ImageNet open dataset was used for pre-training. The pre-trained model is used for further training on the infrared thermal image dataset. This method reduces the requirement of the model for the number of datasets, so that the dataset can be trained quickly and has high detection accuracy. To ensure the fairness of the experiments, we adopted identical training strategies and detection box screening criteria for both models. Specifically, the SSD algorithm was configured with seven prior box scales: (30, 50, 100, 157, 213, 264, 315), a learning rate of 0.0005 during the freezing phase and 0.0001 during the unfreezing phase, and a confidence threshold of 0.5 for retaining detection boxes during inference. The YOLOv5 algorithm strictly adhered to the exact same learning rate schedule and detection criteria as the SSD algorithm.

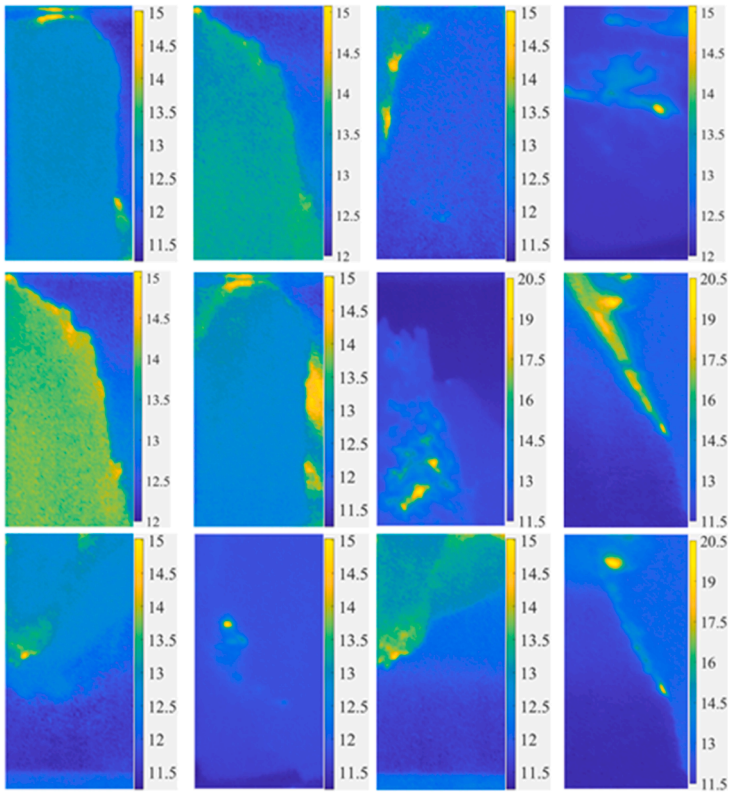

(a) Original infrared thermal image dataset

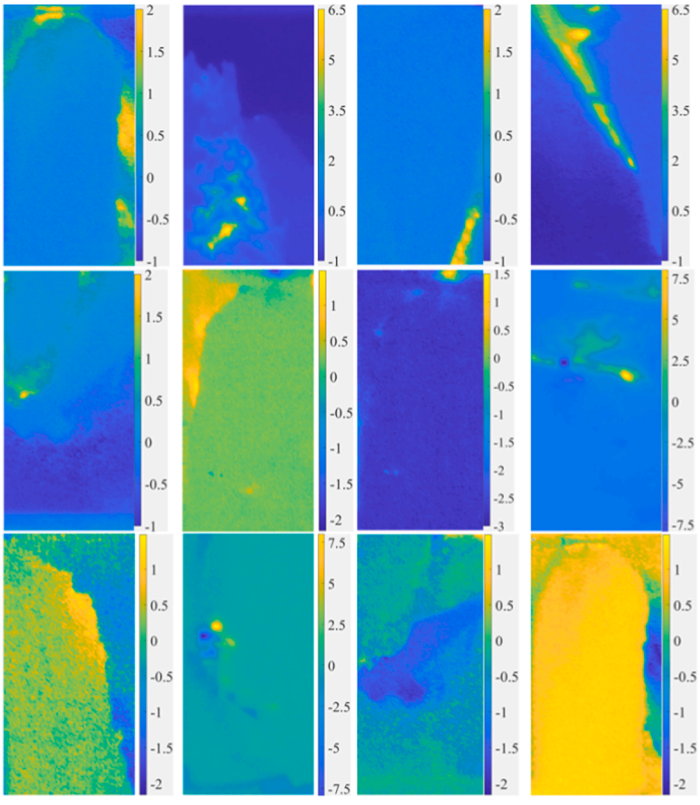

(b) Successive difference infrared thermal image dataset

Fig. 4. Example of infrared thermal image dataset.

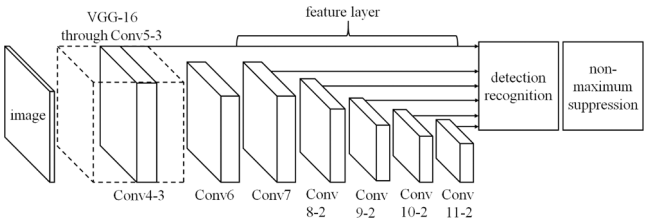

Fig. 5. Structure diagram of SSD algorithm model.

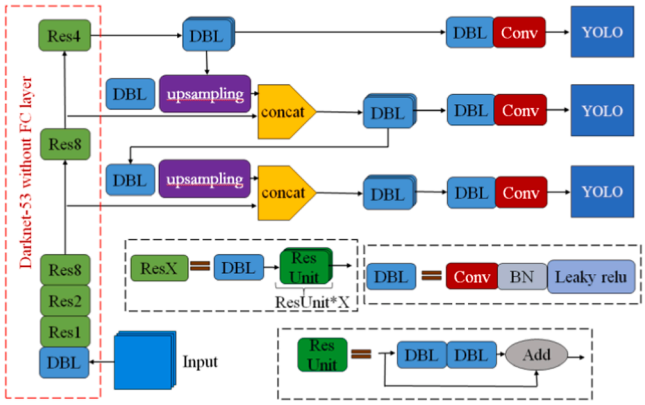

Fig. 6. Structure diagram of YOLOv5 algorithm model.

The process of the model from training to prediction for infrared images is shown in Fig. 7. Infrared image from the dataset was first fed into the backbone network of the deep learning model for feature extraction. Subsequently, the generated crack-specific feature map was propagated to the subsequent modules of the network. The deep learning network model outputs six layers of feature maps with different sizes, on which several default boxes are divided. All feature maps are fed into non-maximum suppression, which selects the default boxes from all feature maps to obtain the output results of the deep learning network model.

3.3. Analysis of training results

As can be seen from the loss function in Fig. 8, the two models have a fast convergence speed during the training process, and with the increase of the number of epochs, the loss value gradually decreases and eventually stabilizes, which indicates that the models can effectively identify the target.

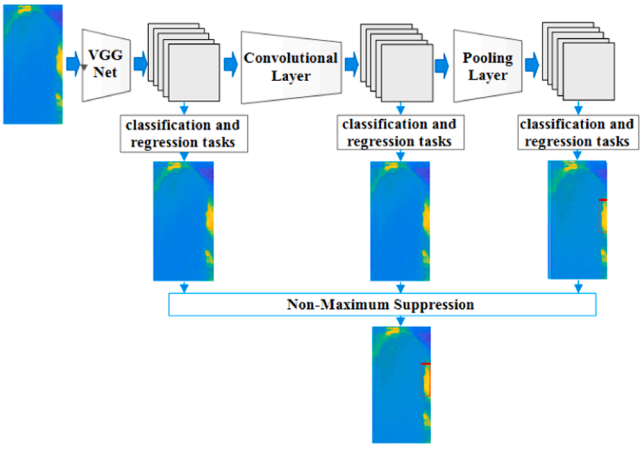

Fig. 7. Sample crack detection procedure.

The SSD and YOLOv5 algorithms were trained on original and successive difference infrared thermal image datasets, respectively, and the training results are shown in Fig. 9. The SSD algorithm can detect more and finer crack groupings, and its confidence level is also significantly improved. When comparing the training results of the two algorithms on the original and successive difference infrared thermal images, it is found that the successive difference infrared thermal images show better training results, with a higher number of detected crack groups, a higher degree of refinement, and a higher confidence level.

The model training results are evaluated using metrics such as mAP, precision, recall, and F1-score, with the corresponding values presented in Table 1. As indicated in Table 1, the successive difference infrared thermal imaging dataset yields better training performance than the original infrared thermal imaging dataset. Specifically, the SSD algorithm trained on the successive difference infrared thermal imaging dataset achieves an mAP of 88.5 %, a recall of 52.8 %, a precision of 96.7 %, and an F1-score of 68.3, outperforming the other three scenarios.

3.4. Analysis of test results

The trained SSD model already has good sandstone crack detection capability; however, whether it can effectively detect the cracks generated during the whole process of loading to rupture of the loading sample still requires a comprehensive inspection of the original, successive difference infrared thermal images of each sample throughout the loading process.

Taking A2 sample as an example, the original infrared thermal image of the whole loading process of the sample is expanded through the methods of angular transformation, flipping and scale transformation, and the original infrared thermal image of the sample is detected by using the SSD algorithm, and the detection results are shown in Fig. 10. The SSD model detected fractures during both the compaction stage and the elastic stage of the specimen, which is inconsistent with the actual situation. This indicates that the model has some degree of misdetection of the original infrared thermal image.

Fig. 11 shows the detection results of the model on the successive difference infrared thermal image of the A2 sample. Compared with the original infrared thermal image, the model has no false detection phenomenon in the detection of the successive difference infrared thermal image and shows a better detection effect.

4. SSD algorithm optimization

The SSD algorithm exhibited poor detection accuracy for small cracks and failed to identify some minor cracks. For this reason, the attention mechanism module was added to the basic network VGG of the original model [25–27].

4.1. Convolutional attention mechanisms

The introduction of this module, Convolutional Attention Mechanism Module (CBAM), enhances the weighting of useful features in subsequent operations and reduces the impact of irrelevantly informative features on the subsequent network model, allowing more representative feature regions to be selected as learning regions for the subsequent network model to focus on. Keeping the SSD algorithm base structure unchanged, two convolutional attention mechanism modules are embedded into the SSD network; one convolutional attention mechanism module is added after Conv4_3 in the backbone feature extraction network, and one convolutional attention mechanism module is added after Conv7 in the additional network structure. After the improvement, the detection image is processed by the added convolutional attention mechanism module to generate a new feature map. The optimized SSD algorithm improves the extraction of important information.

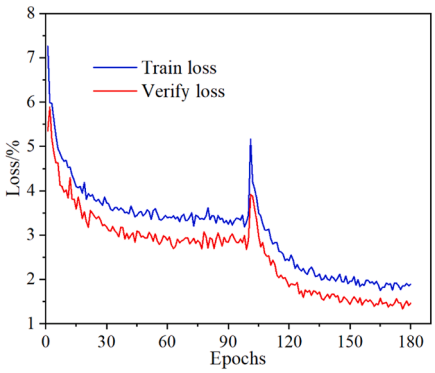

(a) Loss function curves of the original infrared thermal image dataset for SSD algorithm training

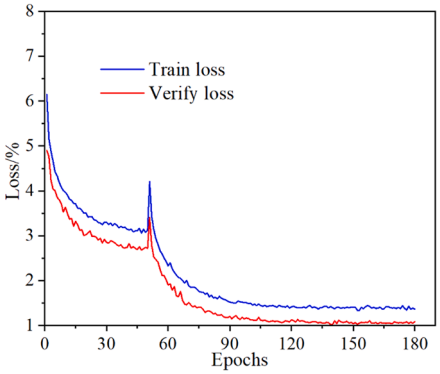

(b) Loss function curves of the differential infrared thermal image dataset for SSD algorithm training

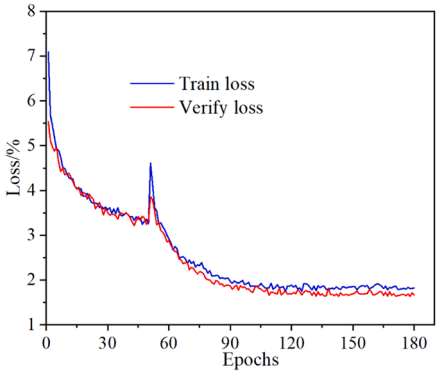

(c) Loss function curves of the original infrared thermal image dataset for YOLOv5 algorithm training

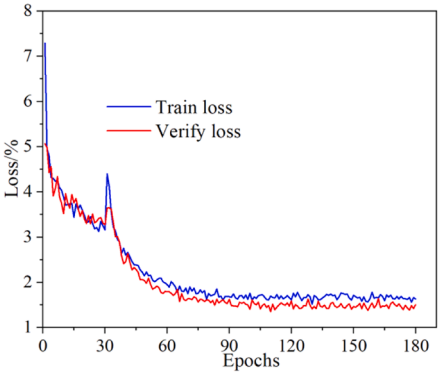

(d) Loss function curves of the successive difference infrared thermal image dataset for YOLOv5 algorithm training

Fig. 8. Loss function curves of the infrared thermal image dataset for the SSD and YOLOv5 algorithm training.

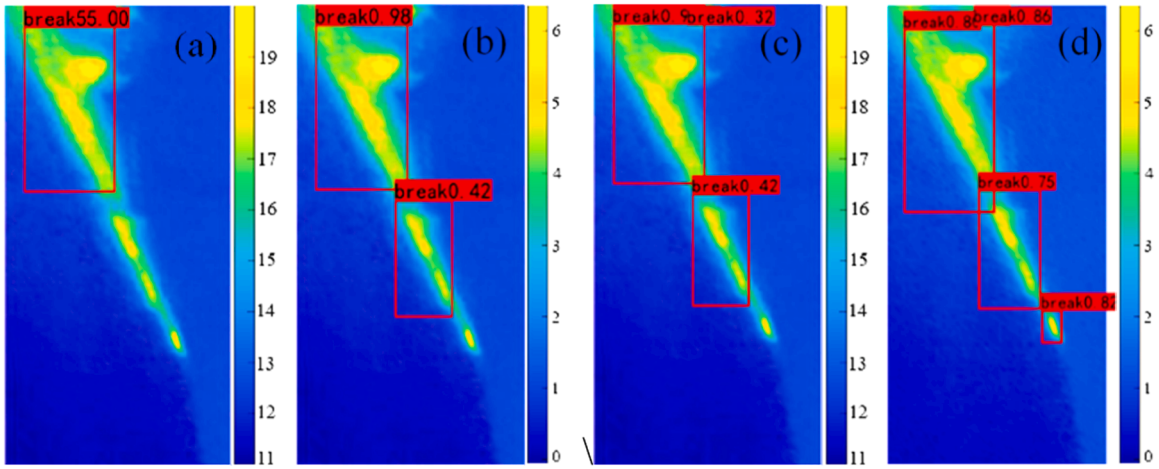

Fig. 9. Comparison of training results between SSD Algorithm and YOLOv5 Algorithm: (a) YOLOv5 processing of original infrared thermal image; (b) YOLOv5 processing of successive difference infrared thermal image; (c) SSD processing of original infrared thermal image; (d) SSD processing of successive difference infrared thermal image.

Table 1
Comparison of evaluation indexes for different models.

Model Category	Infrared thermal image	mAP (%)	Recall (%)	Precision (%)	F1-score (%)
SSD	Original	79.6	51.5	95.7	67.0
	Successive difference	88.5	52.8	96.7	68.3
YOLOv5	Original	63.5	24.1	83.6	37.4
	Successive difference	76.8	42.8	91.37	58.3

4.2. Analysis of optimized model detection results

The successive difference infrared thermal images of the A9 sample were examined using the original SSD algorithm and the optimized SSD algorithm, respectively, and the results are shown in Table 2.

As can be seen from Table 2, the mAP value, recall, precision, and F1-score of the original model for detecting successive difference infrared thermal images are 88.5 %, 52.8 %, 96.7 %, and 68.3 % respectively; for the optimized SSD algorithm in the crack detection of successive difference infrared thermal images, the corresponding mAP value, recall, precision, and F1-score are 90.2 %, 67.1 %, 97.6 %, and 79.6 % respectively. These results indicate that adding the convolutional attention mechanism to the original SSD algorithm has effectively solved the problem of detecting small sandstone cracks. Fig. 12 shows the comparison of the successive difference infrared thermal image detection effect of the A9 sample before and after the optimization of the SSD algorithm, from which it can be clearly seen that, compared with the original SSD algorithm, the optimized algorithm can identify more small crack regions that cannot be identified by the original model, and the detection accuracy is significantly improved.

In addition, in the infrared thermal image after model detection, the area shown by the red box is the temperature increase zone, whose fracture damage form manifests is shear damage, while the green part represents the temperature decrease zone, whose fracture damage form is tensile damage.

5. Conclusions

(1) The dataset of infrared thermal images was constructed, and an infrared thermal image detection model for sandstone cracks based on SSD and YOLOv5 algorithms was established. Compared with the YOLOv5 algorithm, the SSD algorithm can identify the crack region more accurately and has a higher confidence level, and the SSD algorithm has the best crack detection effect in sandstone successive difference infrared thermal images with better accuracy and generalization ability.

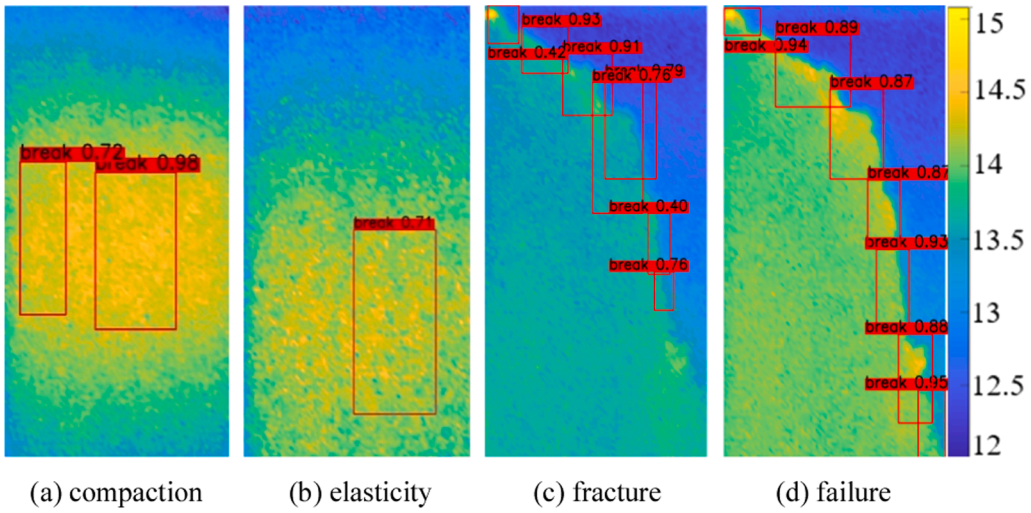

Fig. 10. Test results of the original infrared thermal image model of sample A2.

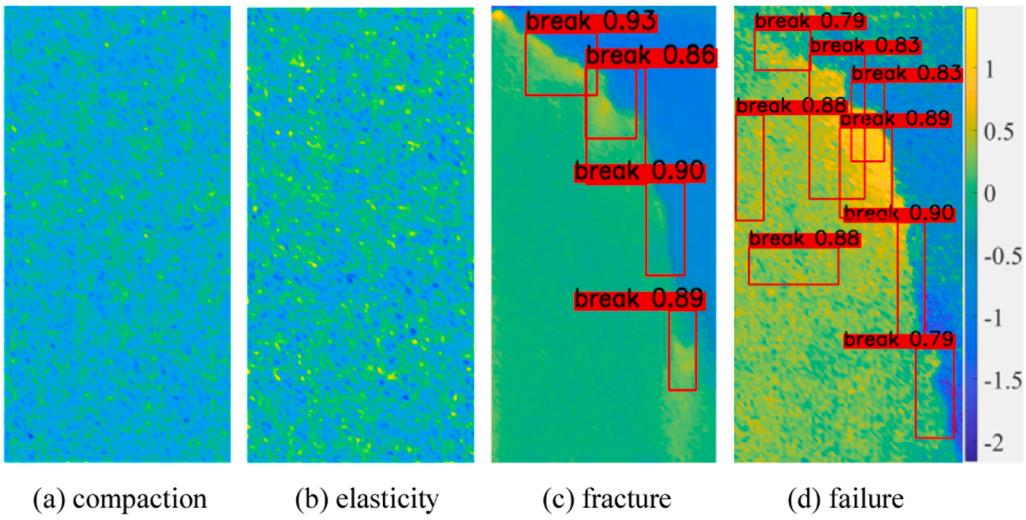

Fig. 11. Test results of successive difference infrared thermal image model of sample A2.

Table 2
Comparison of detection results before and after SSD algorithm optimization.

Model Category	Infrared thermal image	mAP (%)	Recall (%)	Precision (%)	F1-score (%)
Original model	Successive difference	88.5	52.8	96.7	68.3
Optimization models	Successive difference	90.2	67.1	97.6	79.6

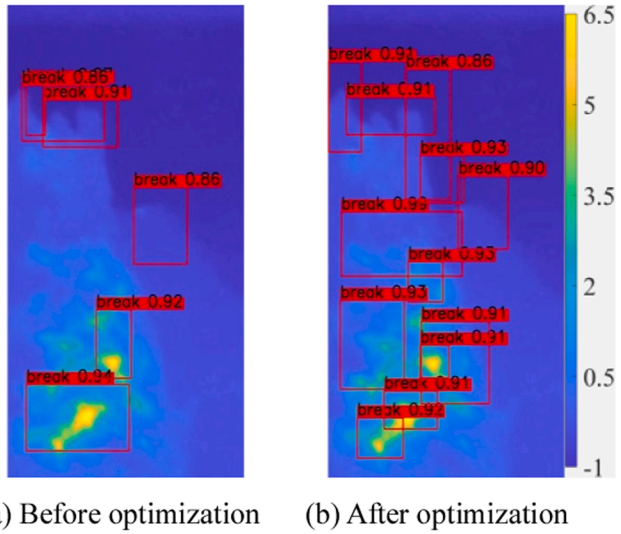

Fig. 12. Comparison of test results of sample A9 before and after model optimization.

(2) The mAP values after training on the original infrared thermal image and successive difference infrared thermal image dataset are 79.6 % and 88.5 %, respectively, and the sandstone crack infrared thermal image detection model based on the SSD algorithm has the ability of sandstone crack detection, and it has a better detection effect on the successive difference infrared thermal image.

(3) By introducing the convolutional attention mechanism, the SSD algorithm achieved a mAP value of 90.2 % for detecting cracks in successive difference infrared thermal images, enhancing sandstone crack detection accuracy.

Authors' contributions

All authors contributed to the study conception and design. Material preparation, data collection and analysis were performed by Hai Sun. The first draft of the manuscript was written by Hai Sun, and all authors commented on previous versions of the manuscript. All authors read and approved the final manuscript.

CRediT authorship contribution statement

Hai Sun: Writing – review & editing, Writing – original draft. **Xinyi Hou:** Data curation. **Liqiang Ma:** Formal analysis. **Wenshuang Gao:** Data curation. **Kun Wang:** Methodology.

Declaration of Competing Interest

The authors declare that they have no known competing financial interests or personal relationships that could have appeared to influence the work reported in this paper.

Acknowledgments

This article was supported by the Project of Liaoning Provincial Department of Education (JYTMS20231458), Xinjiang Key Laboratory of Green Mining of Coal resources, Ministry of Education (KLXGY-KB2402), the National Natural Science Foundation of China (52464015) and the Talent Introduction Scientific Research Start-up Foundation of Liaoning Petrochemical University (2019XJJL-025).

Data availability statement

All data included in this study are available upon request by contact with the corresponding author.

References

[1] L. Yuan, E.Y. Wang, Y.K. Ma, et al., Research progress of coal and rock dynamic disasters and scientific and technological problems in China, J. China Coal Soc. 48 (5) (2023) 1825–1845.
[2] J.X. Zhang, J.Y. Wang, N. Zhou, et al., Collaborative mining system of geothermal energy and coal resources in deep mines, Chin. J. Eng. 44 (10) (2022) 1682–1693.
[3] Q. Sun, X.H. Xue, S.Y. ZHU, The identification method of critical information for rock brittle failure, Chin. J. Solid Mech. 34 (3) (2013) 311–319.
[4] T.W. Lan, Z.J. Zhang, Y.N. Yuan, et al., An evaluation method for geological dynamic environments of mines and the classification of mines subjected to rock bursts, Coal Geol. Explor. 51 (2) (2023) 104–113.

[5] K.G. Zheng, L.T. Wang, B.G. Li, et al., Dynamie disaster evolution mechanism of high mine pressure at hard roof and advance area prevention and control technology, Coal Geol. Explor. 50 (8) (2022) 62–71.
[6] L.X. Wu, J.Z. Wang, Infrared thermal image and radiation temperature characteristic experiment of coal rock under compression, Sci. China(Ser. D : Earth Sci.) 28 (1) (1998) 41–46.
[7] L.X. Wu, J.Z. Wang, Study on thermal infrared radiation themperature omen in coal-measure rock yielding under ground pressure, China Min. Mag. 6 (6) (1997) 42–48.
[8] L.X. Wu, S.J. Liu, Y.H. Wu, et al., Remote-sensing-rock mechanics(IV)——Laws of thermal infrared radiation from compressively-sheared fracturing of rock and its meanings for earthquake omens, Chin. J. Rock Mech. Eng. 23 (4) (2004) 539–544.
[9] S.J. Liu, L.X. Wu, C.Y. Wang, et al., Remote sensing-rock mechanics(VIII)——TIR omens of rock fracturing, Chin. J. Rock Mech. Eng. 23 (10) (2004) 1621–1627.
[10] Z.H. Li, H. Tian, Y. Niu, et al., Study on the acoustic and thermal response characteristics of coal samples with various prefabricated crack angles during loaded failure under uniaxial compression, J. Appl. Geophys. 200 (2022) 104618.
[11] X.Z. Wu, X. Gao, K. Zhao, et al., Abnormality of transient infrared temperature field (ITF) in the process of rock failure, Chin. J. Rock Mech. Eng. 35 (8) (2016) 1578–1594.
[12] L.Q. Ma, D.S. Zhang, X.W. Guo, et al., Characteristics on the variance of differential pressurised sequence during coal failures under coal failures under uniaxial loading, Chin. J. Rock Mech. Eng. 36 (S2) (2017) 3927–3934.
[13] X.F. Liu, Y.Q. ZHAO, X.R. Wang, et al., Current status and prospects of research on fatigue damage and failure precursors of rocks, Earth Sci. 47 (6) (2022) 2190–2198.
[14] Zi.L. Zhou, Y. Liu, X. Cai, et al., Infrared radiation characteristics of sandstone exposed to impact loading, J. Central South Univ.(Sci. Technol.) 53 (7) (2022) 2555–2562.
[15] Q.H. Zhang, C. Chen, L. Yuan, et al., Early and intelligent recognition of dynamic cracks during damage of complex fractured rock masses based on DIC and YOLO algorithms, J. China Coal Soc. 47 (3) (2022) 1208–1219.
[16] X.Y. Xu, M. Zhao, P.X. Shi, et al., Crack detection and comparison study based on faster R-CNN and mask R-CNN, Sensors 22 (2022) 1215.
[17] Y.X. Yuan, N. Zhang, C.L. Han, et al., Automated identification of fissure trace in mining roadway via deep learning, J. Rock Mech. Geotech. Eng. 15 (8) (2023) 2039–2052.
[18] Y. Lu, Rock thermal infrared image tension-shear crack detection based on deep learning, M.S. Thesis, North China University of Science and Technology, 2022.
[19] X.H. Huang, T.F. Li, X.X. Liu, et al., Research on tracking and prediction of rock fissure sevelopment based on improved Faster R-CNN algorithm, J. Henan Polytechnic Univ.(Nat. Sci.) 41 (4) (2022) 134–141.
[20] K. Jang, N. Kim, Y.K. An, Deep learning-based autonomous concrete crack evaluation through hybrid image scanning, Struct. Health Monit. 18 (2019) 1722–1737.
[21] M.Q. Li, Research on infrared object detection algorithm based on deep learning, M.S. Thesis, Xidian University, 2022.
[22] C. Chen, Research on damage testing and fracture detection and identification of complex fractured rock masses, M.S. Thesis, Anhui University of Science and Technology, 2022.
[23] X.H. Zhao, T.Y. Che, S. Ye, et al., Segmentation method of the abnormal area of coal infrared thermal image, J. Mine Autom. 48 (2022) 92–99.
[24] M.Z. Zhang, J.Z. Duan, Z.W. Liang, et al., Fire and smoke detection method based on improved YOLO-V5 algorithm, China Saf. Sci. J. 34 (5) (2024) 155–161.
[25] J. Li, D.Y. Lin, Y. Wang, et al., Deep discriminative representation learning with attention map for scene classification, Remote Sens. 12 (2020) 1366.
[26] B. Gianni, F. Flavius, A general survey on attention mechanisms in deep learning, IEEE Trans. Knowl. Data Eng. 35 (4) (2021) 3279–3298.
[27] C.L. Tang, D. Zhang, Q.C. Tian, Convolutional neural network–bidirectional gated recurrent unit facial expression recognition method fused with attention mechanism, Appl. Sci. 13 (2023) 12418.

Hai Sun is an Associate Professor of School of Civil Engineering, Liaoning Petrochemical University, Fushun, China. His research expertise includes rock mass stability analysis, remote sensing rock mechanics and geotechnical engineering.